AGU PUBLICATIONS

Geophysical Research Letters

RESEARCH LETTER
10.1002/2017GL073336

Key Points:
- Changes in wintertime Pacific (PA) and Euro-Atlantic (EA) blocking frequencies depend on strength and types of El Niño, respectively
- Wintertime PA and EA blocking frequency decreases (increases) by 1.7% to 7.1% (0.7%) and 2.6% to 5.8% (0.4%), respectively
- Summertime EA blocking frequency shows a robust decrease by 2.4% to 4.1%. Long-lasting blocking events show a less robust decrease

Supporting Information:
- Supporting Information S1

Correspondence to:
M. Matsueda,
mio@ccs.tsukuba.ac.jp

Citation:
Matsueda, M., and H. Endo (2017), The robustness of future changes in Northern Hemisphere blocking: A large ensemble projection with multiple sea surface temperature patterns, *Geophys. Res. Lett.*, *44*, doi:10.1002/2017GL073336.

Received 4 MAR 2017
Accepted 13 MAY 2017
Accepted article online 16 MAY 2017

The robustness of future changes in Northern Hemisphere blocking: A large ensemble projection with multiple sea surface temperature patterns

Mio Matsueda[1,2] and Hirokazu Endo[3]

[1]Center for Computational Sciences, University of Tsukuba, Tsukuba, Japan, [2]Department of Physics, University of Oxford, Oxford, UK, [3]Meteorological Research Institute, Tsukuba, Japan

Abstract Future changes in the frequency of Northern Hemisphere blocking are investigated via large ensemble simulations using a 60 km mesh atmospheric general circulation model prescribed with six future sea surface temperature patterns derived from state-of-the-art climate models under a 4 K warmer climate. Our simulations depict the frequency of wintertime blocking decreasing from 16.6% ± 0.7% to 13.1% ± 2.1% in the Euro-Atlantic sector and from 17.4% ± 0.7% to 14.8% ± 2.4% in the Pacific sector. This decline in frequency is seen to affect Euro-Atlantic blocking of all durations and Pacific blocking of more than 15 days' duration. During summer, our simulations not only exhibit a robust decrease (from 10.7% ± 0.4% to 7.6% ± 0.7%) in the Euro-Atlantic blocking frequency but also show that the magnitude of this decrease is smaller for longer-lived blocking. In contrast, the Pacific blocking frequency either does not change or increases slightly, particularly for events of 15–29 days' duration.

1. Introduction

Atmospheric blocking (an anticyclonic quasi-stationary flow pattern) is a fundamental characteristic of midlatitude weather and climate, and persistent blocking events can induce extreme temperature and precipitation anomalies over a large geographic area [e.g., *Black et al.*, 2004; *Matsueda*, 2011]. Although general circulation models (GCMs) typically underestimate the frequency of blocking in climate simulations [e.g., *D'Andrea et al.*, 1998; *Palmer et al.*, 2008, *Anstey et al.*, 2013; *Masato et al.*, 2013], a number of more recent GCMs, including those of the intercomparison projects, e.g., the first Atmospheric Model Intercomparison Project (AMIP1, 1992), phase 3 of the Coupled Model Intercomparison Project (CMIP3 [*Meehl et al.*, 2007]), and phase 5 of the Coupled Model Intercomparison Project (CMIP5 [*Taylor et al.*, 2012]), have made significant improvements in simulating blocking frequency, particularly over the Pacific sector [*Intergovernmental Panel on Climate Change (IPCC)*, 2013; *Davini and D'Andrea*, 2016].

State-of-the-art high-resolution atmospheric GCMs (AGCMs) are showing improved simulations of the frequency of blocking, especially over the Euro-Atlantic sector, attributed to an increase in the horizontal and vertical resolutions of models [e.g., *Matsueda et al.*, 2009, 2010; *Jung et al.*, 2012; *Anstey et al.*, 2013; *Schiemann et al.*, 2017]. These AGCMs can provide more reliable projections of blocking events and blocking-related regional climate change, such as heatwaves, cold snaps, and large-scale extreme rainfall, than do the more typical, coarser-resolution climate models. For example, using initial-value ensemble simulations of the Japan Meteorological Agency Meteorological Research Institute's high-resolution Atmospheric GCM (MRI-AGCM3.1), *Matsueda et al.* [2009] projected that the frequency of Northern Hemisphere wintertime blocking will decrease significantly by the end of the 21st Century. In that study, the MRI-AGCM3.1 was perturbed with CMIP3 multimodel ensemble mean sea surface temperature (SST), in keeping with other studies using the coarser-resolution CMIP models [e.g., *Masato et al.*, 2013].

Although the CMIP5 models are demonstrably better at simulating blocking events than the AMIP and CMIP3 models, CMIP5 simulations nonetheless underperform relative to the MRI-AGCM regarding the frequency of blocking [*Davini and D'Andrea*, 2016; *Matsueda et al.*, 2009] and considerable disparity exists in projected SSTs, particularly at the equator. Furthermore, the atmospheric response (i.e., teleconnection) to SST is thought to be strongly model-dependent. Tropical SSTs, particularly in the Pacific Ocean, can have a significant impact on midlatitude climate, with this effect being most pronounced during winter [e.g., *Palmer and*

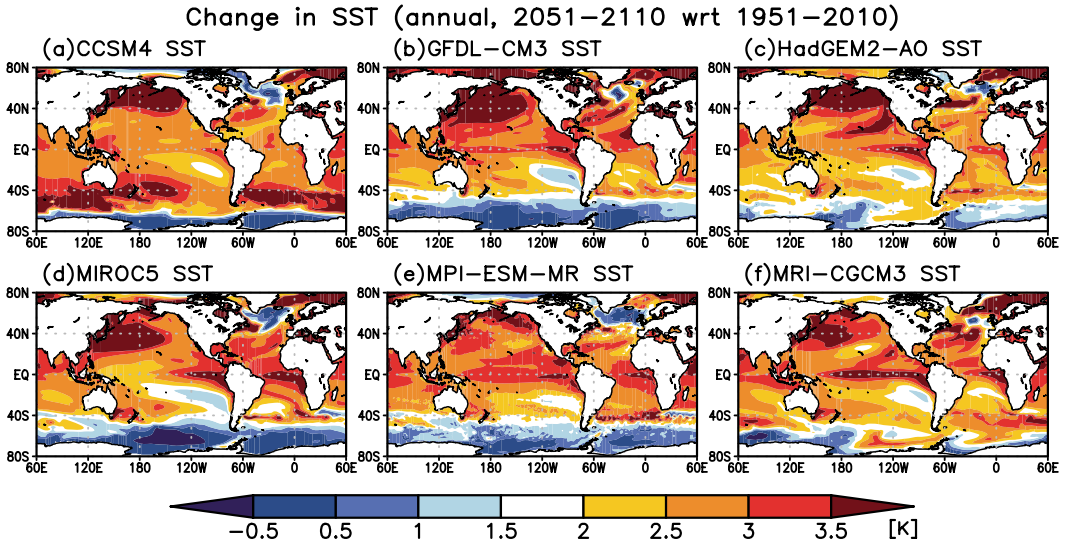

Figure 1. Prescribed changes in annual-mean SST for the period 2051–2110 relative to 1951–2010: (a) CCSM4, (b) GFDL-CM3, (c) HadGEM2-AO, (d) MIROC5, (e) MPI-ESM-MR, and (f) MRI-CGCM3.

Mansfield, 1984; *Trenberth et al.*, 2014]. Consequently, large uncertainties in the projected distribution and amplitude of tropical Pacific SSTs, coupled with the model-dependent atmospheric response to these projections, may produce sizable uncertainties in the frequency of simulated blocking events and related atmospheric phenomena in a warming climate [*IPCC*, 2013, chapter 14].

In this study, we describe ensemble simulations made using a high-resolution MRI-AGCM to investigate the robustness of future changes in Northern Hemisphere blocking under various sea surface conditions. Our model is forced with SST projections from CMIP5, assuming a climate warming of 4 K relative to preindustrial conditions.

2. Methodology

The large ensemble data sets from the experiments described here are available on the Database for Policy Decision Making for Future Climate Change (d4PDF [*Mizuta et al.*, 2017]).

2.1. Model, Model Experiments, and Observations

The AGCM used here (hereafter, MRI-AGCM3.2) was developed by MRI in Japan [*Mizuta et al.*, 2012]. The horizontal resolution of the MRI-AGCM3.2 is 0.56° × 0.56° (T_L 319, 40 km at 50°N) in latitude and longitude, with 64 vertical levels (top at 0.01 hPa).

We conducted model integrations for a 60 year historical climate (1951–2010) and a 60 year future climate (2051–2110), in which global-mean surface air temperature becomes 4 K (3.6 K) warmer than the preindustrial (historical) climate. The SST, sea ice concentration, and sea ice thickness (SIT) were each prescribed as lower boundary conditions. For the historical climate, we applied different arbitrary initial conditions and small SST perturbations (δSSTs, their amplitude is set to be 30% of the standard deviation of the interannual SST variability) to 100-member ensemble simulations prescribed with observed monthly mean SST and SIC (COBE-SST2 [*Hirahara et al.*, 2014]) and climatological monthly SIT [*Bourke and Garrett*, 1987] as lower boundary conditions.

In the +4 K climate simulations, we kept the amplitude of warming constant throughout the 60 year integration to obtain a large sample size under a specific stage of global warming. This stage corresponds to the end of the 21st Century under the CMIP5 Representative Concentration Pathway 8.5 (RCP8.5) scenario. Using six CMIP5 models (CCSM4, GFDL-CM3, HadGEM2-AO, MIROC5, MPI-ESM-MR, and MRI-CGCM3), we calculated climatological SST warming patterns (ΔSSTs) as differences between the periods 2080–2099 and 1991–2010 in both the historical and RCP8.5 experiments (Figure 1). These models were selected through cluster analysis of

geographical patterns in SST change, which indicated that these patterns account for most of the SST uncertainty in all CMIP5 models [*Mizuta et al.*, 2014]. All the SST warming patterns, except the MRI-CGCM3 SST pattern, include the canonical eastern Pacific El Niño signal (the MIROC5 (CCSM4) SST pattern shows the strongest (weakest) signal), whereas the MRI-CGCM3 SST pattern does the central Pacific (CP) El Niño signal rather than the canonical Pacific El Niño signal. Warming patterns (ΔSSTs) were then applied to the observed SST record, from which the long-term trend had been removed. Finally, we conducted 15-member ensemble simulations for each of the six future SST patterns using different arbitrary initial conditions and δSSTs under the 2090 levels of greenhouse gas concentrations anticipated in the RCP8.5 scenario.

To assess the model's performance in simulating the frequency and duration of blocking events for the period 1951–2010, we used 500 hPa geopotential height (Z500) data from the 55 year Japanese reanalysis [JRA55; *Kobayashi et al.*, 2015].

2.2. Blocking Index and Duration

Following *Matsueda et al.* [2009], we employed the objective blocking index proposed by *D'Andrea et al.* [1998]. Specifically, the Z500 meridional gradients, GHGS and GHGN, are computed for each longitude as follows:

$$\begin{cases} \mathrm{GHGS} = \dfrac{Z(\varphi_0) - Z(\varphi_s)}{\varphi_0 - \varphi_s}, \\ \mathrm{GHGN} = \dfrac{Z(\varphi_n) - Z(\varphi_0)}{\varphi_n - \varphi_0}, \end{cases}$$

where

$$\begin{cases} \varphi_n = 77.5^{\circ}N \pm \Delta \\ \varphi_0 = 60.0^{\circ}N \pm \Delta \\ \varphi_s = 40.0^{\circ}N \pm \Delta \end{cases}, \quad \Delta = 0^{\circ}, 1.25^{\circ}, 2.5^{\circ}, 3.75^{\circ}, 5.0^{\circ}.$$

A specific longitude on a given day is locally defined as being blocked ("local blocking") if both of the following conditions are satisfied (for at least one value of Δ):

$$\begin{cases} \mathrm{GHGS} > 0, \\ \mathrm{GHGN} < -5 \ \ \mathrm{m/(deglat)}. \end{cases}$$

To calculate the duration of blocking, "sector blocking" is also defined. The Euro-Atlantic and Pacific sectors are defined using the longitudinal limits of 60°W–40°E and 100°E–120°W, respectively. Sector blocking is then defined as the simultaneous blocking of three or more adjacent longitudes within the sector limits relative to the previous local index definition.

The duration is calculated for sector blocking using a loose time-continuity constraint. For instance, in the case that two consecutively blocked days in a sector are followed by a nonblocked day and then two more consecutively blocked days, the entire 5 day period is considered as a single blocking event. An analogous criterion is applied to the case that a single nonblocked day is preceded (followed) by three blocked days and is followed (preceded) by a single blocked day.

The Student's *t* test for difference of means is used to determine whether future change in the blocking frequency and duration is significant.

3. Results

Although the MRI-AGCM3.2 (1951–2010) exhibits several biases in simulations of DJF (December–February) and JJA (June–August) blocking frequency against JRA55 (1958–2010), we note that the MRI-AGCM3.2 in general simulates the locations of the local maxima and minima of the blocking frequency well (Figure 2). Our simulations project that the frequencies of Euro-Atlantic and Pacific blocking in DJF will decrease significantly over the western tail of both sectors, a pattern that is evident in most of the ΔSST ensemble simulations (Figures 2a and 2b). We also observed a significant and robust increase in frequency over the eastern tail of

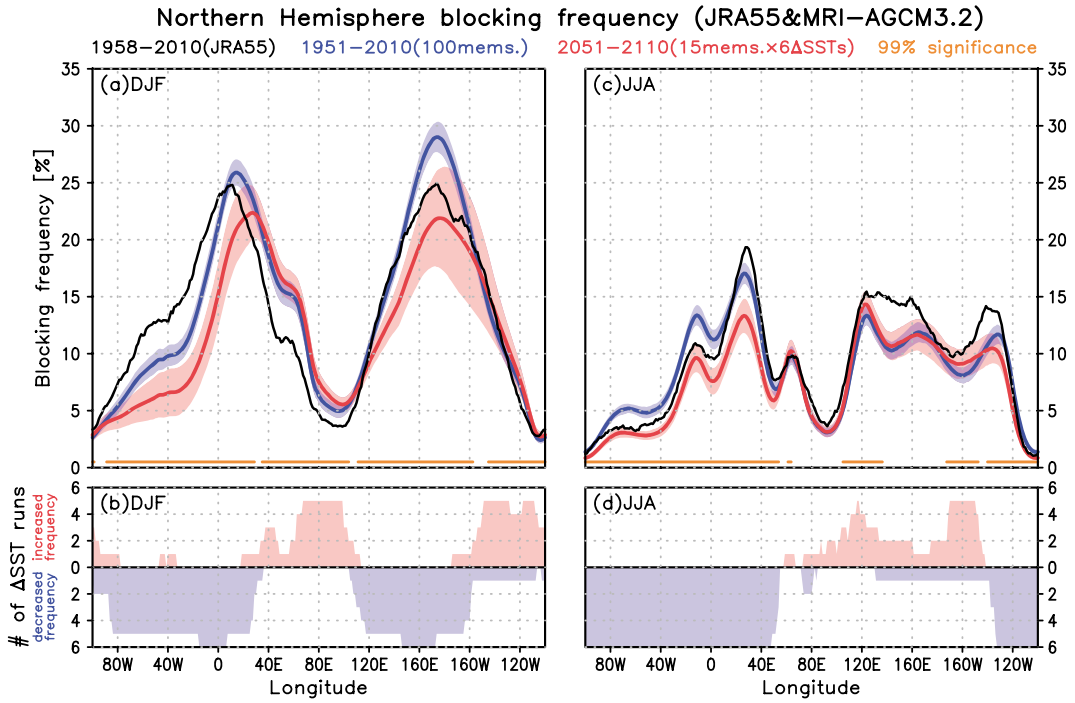

Figure 2. Ensemble-mean frequency of blocking in (a) winter and (c) summer in the Northern Hemisphere as a function of longitude for JRA55 (black, 1958–2010) and the ensemble simulations perturbed with COBE-SST2 (blue, 1951–2010) and six ΔSSTs (red, 2051–2110). The red and blue shading represent the ±1 standard deviation of the blocking frequency for the periods 1951–2010 and 2051–2110, measured from 100- and 90-ensemble members, respectively. The orange bars indicate the longitudes for which the future change in the blocking frequency is significant at the 99% confidence level. Also shown is the number of ΔSST ensemble simulations in (b) winter and (d) summer for which the 15-member mean blocking frequency for 2051–2110 shows a significant (at the 99% confidence level) increase (red) or decrease (blue) relative to the corresponding 100-member mean frequency for the period 1951–2010.

each peak, suggesting a slight eastward shift in the frequency of blocking, although we note that the change in absolute value is considerably smaller here than over each peak and respective western tail.

There are some important differences in the wintertime frequency changes among the ΔSST simulations (Figure S1 in the supporting information). For example, the MRI-CGCM3 (CCSM4) SST-forced simulation exhibits significant changes in blocking frequency over less-extensive Euro-Atlantic (Pacific) sectors compared with the other simulations, and the pattern of Z500 change in these runs is also markedly different (Figure S2). Specifically, the MRI-CGCM3 SST distribution shows a distinct southwestward shift in the Euro-Atlantic Z500 minimum that resembles the response of 1000 hPa geopotential height to the CP El Niño, a linkage that is facilitated by the "stratospheric bridge" (Figure 3 in *Graf and Zanchettin* [2012]). Indeed, the El Niño signal in the prescribed MRI-CGCM3 SST (Figure 1f) is closer to the CP El Niño than to the canonical eastern Pacific El Niño. We also note that the peaks in rainfall and strong tropical convection, measured as 200 hPa velocity potential, also shift westward in this run compared with the other simulations (Figure S3).

Concurrently, the CCSM4 SST-forced simulation exhibits the weakest meridional Z500 gradient over the Pacific sector (Figure S2a), which we attribute to the weak El Niño signal. In contrast, the MIROC5 SST-forced simulation, for which the El Niño signal is the strongest of all prescribed SSTs, displays the largest frequency reductions over both the Euro-Atlantic and Pacific sectors (Figure S1), due to the largest meridional Z500 gradients of all our experiments (Figure S2).

Under canonical El Niño SST conditions, the frequency of blocking averaged over the Euro-Atlantic sector (hereafter areal-mean frequency) in DJF (column 2 in Table 1) declines considerably by between 2.6% (HadGEM2-AO SST) and 5.8% (MIROC5 SST). In contrast, under CP El Niño-type SST conditions, these values increase slightly (0.4%, MRI-CGCM3 SST). For each ensemble simulation the standard deviation of the frequencies is <1.0. The reduced frequency of Euro-Atlantic blocking is possible even under the CP El

Table 1. Areal-Mean Frequencies (%) of Simulated Blocking Events and Their Standard Deviations Measured by Ensemble Spread for the Euro-Atlantic (60°W–40°E, Columns 2 and 4) and Pacific Sectors (100°E–120°W, Columns 3 and 5) in DJF and JJA for Each ΔSST Ensemble Simulation[a]

	DJF		JJA	
	Euro-Atlantic	Pacific	Euro-Atlantic	Pacific
1951–2010 (100)	16.6 ± 0.7	17.4 ± 0.7	10.7 ± 0.4	10.1 ± 0.4
2051–2110 (90, all SSTs)	13.1 ± 2.1▼	14.8 ± 2.4▼	7.6 ± 0.7▼	10.2 ± 0.9
(15, CCSM4 SST)	12.5 ± 0.7▼	18.1 ± 0.7●	7.4 ± 0.5▼	10.7 ± 0.3●
(15, GFDL-CM3 SST)	12.3 ± 1.0▼	15.3 ± 0.5▼	7.8 ± 0.4▼	11.1 ± 0.5●
(15, HadGEM2-AO SST)	14.0 ± 0.5▼	14.5 ± 0.5▼	8.3 ± 0.4▼	10.2 ± 0.5
(15, MIROC5 SST)	10.8 ± 0.7▼	10.3 ± 0.5▼	6.6 ± 0.4▼	8.7 ± 0.4▼
(15, MPI-ESM-MR SST)	11.7 ± 0.8▼	14.8 ± 0.4▼	7.8 ± 0.5▼	10.5 ± 0.4●
(15, MRI-CGCM3 SST)	17.0 ± 0.5	15.7 ± 0.7▼	7.9 ± 0.5▼	10.2 ± 0.5

[a]The numbers in parentheses (column 1) denote the ensemble size in each ΔSST simulation. The triangles (▼) and circles (●) denote significantly (at the 99% confidence level) decreased and increased blocking frequencies, respectively, for the period 2051–2110 relative to 1951–2010.

Niño-type SST warming. Reduction rates for DJF in the Pacific sector (column 3) vary considerably from 1.7% (MRI-CGCM3 SST) to 7.1% (MIROC5 SST) on average. We observed that although the frequency of Pacific blocking increases by 0.7% during weak El Niño-type SST warming (i.e., CCSM4 SST), most of the simulations show this frequency declining.

In the Euro-Atlantic sector during DJF, the number of blocking events in each 5 day category is projected to decrease significantly regardless of the overall duration of blocking (Figure 3a). One exception is the MRI-CGCM3 SST-forced simulation, which exhibits no significant decrease in the number of blocking events but shows a significant increase in the number of events of 20–24 days' duration (not shown). Our simulations also project significant and robust reductions in the number of blocking events over the Pacific, but only for events of $>$15 days' duration (Figure 3b). For those lasting 5–9 days, we observed a significant but non-robust increase, whereas events of 10–14 days' duration decreased in number. None of the simulations projected a decrease in the number of 5–9 day blocking events.

For the JJA period, all ensemble runs depict significant and robust decreases in the frequency of Euro-Atlantic blocking events west of 40°E, whereas only the MPI-ESM-MR SST-forced simulation projects a significant increase in Ural blocking (40°–80°E, Figures 2c and 2d and S4). The greatest reduction in Euro-Atlantic blocking frequency occurs in the MIROC5 SST-forced simulation (Figure S4), which also depicts the largest decrease in wintertime blocking. In contrast, the smallest frequency reductions are projected by the HadGEM2-AO-forced simulation. On average, the areal-mean frequency of Euro-Atlantic blocking events is shown to decline by between 2.4% (HadGEM2-AO SST) and 4.1% (MIROC5 SST), with standard deviations being uniformly $<$0.5 (Table 1). Taken together, these results suggest that the frequency of summer blocking events in the Euro-Atlantic sector is unlikely to increase. Indeed, the number of JJA events lasting up to 24 days exhibits a significant and robust decrease, while events of $>$25 days' duration show a significant but less robust decrease (Figure 3c). In summary, the longer the blocking duration, the less robust the projected decrease in the number of events.

In the Pacific sector, the frequency of summertime blocking remained unchanged or increased slightly, indicating the weaker robustness of the projected response compared with other sectors (Figures 2c and 2d). In addition, the absolute values of any changes are significantly smaller than those in the Euro-Atlantic sector. The largest reduction in Pacific frequency, in particular east of 140°E, is exhibited by the MIROC5 SST-forced simulation (Figure S4). In contrast, both the CCSM4 SST- and GFDL-CM3 SST-forced simulations show increased frequencies of Pacific blocking. Enhanced blocking is also evident around 120°E in the MIROC5 SST- and MPI-ESM-MR SST-forced runs and around 160°W in the runs forced with HadGEM2-AO, MPI-ESP-MR, and MRI-CGCM3 SSTs.

Taken together, these results suggest that the areal-mean frequency of Pacific blocking may either increase on average by between 0.4% (MPI-ESM-MR SST) and 1.0% (GFDL-CM3 SST) or decrease by as much as 1.4% (MIROC5 SST) (Table 1). The other simulations in our experiment do not project any significant change in the areal-mean blocking frequency for this sector. Therefore, our findings suggest that simulated changes in

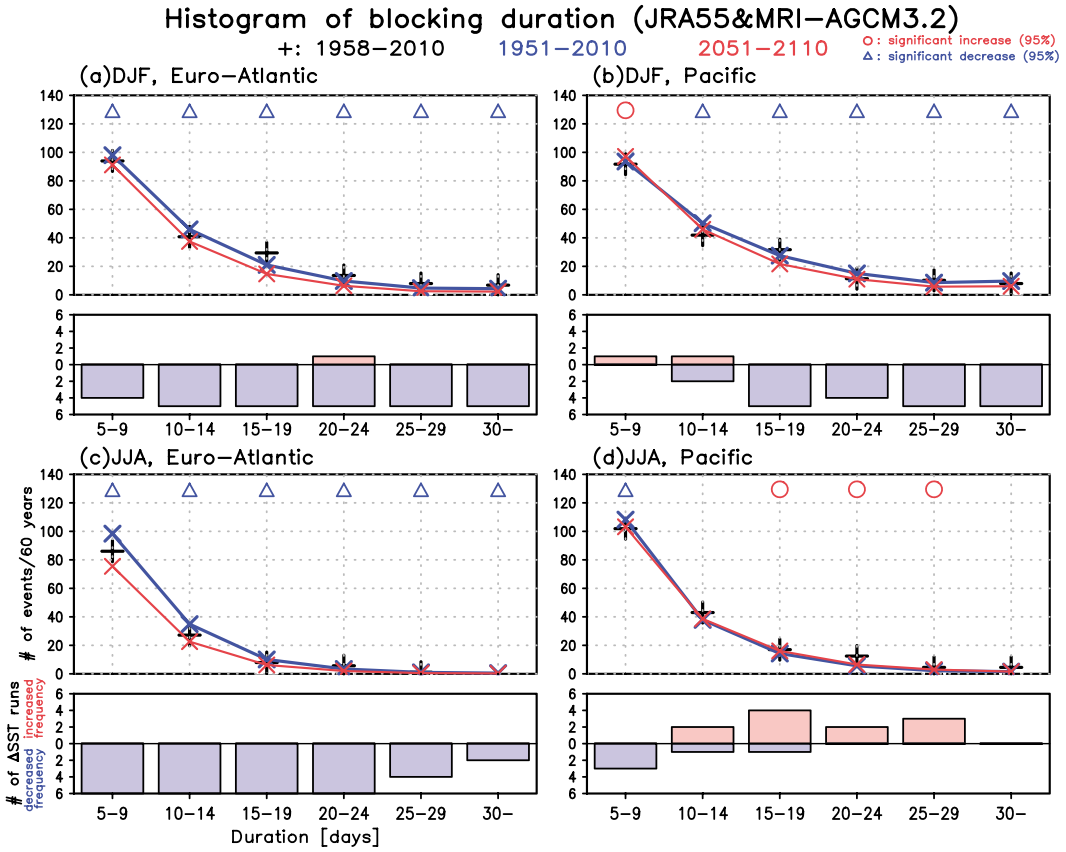

Figure 3. Histogram of the durations of observed (plus symbols) and simulated (solid lines with multiplication symbols) blocking events over the Euro-Atlantic and Pacific sectors in (a and b) winter and (c and d) summer for the periods 1958–2010 (JRA55, black), 1951–2010 (100 members, blue), and 2051–2110 (15 × 6 members, red). The number of events for JRA55 (53 year data) is rescaled by 60/53 to enable comparison with the 60 year simulations. The red circles and blue triangles indicate significant changes in the number of blocking events for each 5 day duration bin at the 95% confidence level. The red and blue bars indicate the number of the ΔSST ensemble simulations for which the 15-member mean number of blocking events shows a significant increase or decrease, respectively, at the 95% confidence level.

frequency are largely uncertain. In a warming climate, Pacific blocking events lasting 15–29 days are projected to occur more frequently and those lasting 5–9 days less frequently (Figure 3d). Most of these projected changes are moderately robust (i.e., three to four of six ensemble simulations show a significant change).

In summary, we emphasize that the response of blocking activity to global warming in the Pacific sector differs markedly among sectors and seasons, suggesting the influence of additional mechanisms. For example, *Arai and Kimoto* [2008] suggested that global warming will enhance the land-sea thermal contrast, resulting in increased blocking events over eastern Siberia.

Finally, more detailed future changes in the blocking frequency are shown with Hovmöller diagram (Figure 4). In the Euro-Atlantic sector, the ensemble simulations show significant decreases in the frequency of blocking throughout the year. Furthermore, with the exception of the prime meridian region during late winter-midspring, each ΔSST ensemble simulation indicates that the most pronounced decreases reflect robust changes. The largest reduction in blocking frequency occurs on the prime meridian in February. Only the MRI-CGCM3 SST-forced simulation shows no significant change in blocking frequency in that region at the 99% confidence level (Figure S5), resulting in a weaker robustness.

Over the Ural sector, pronounced increases in frequency are projected east of 60°E from March to June and over most of the sector from October to January, although the latter are only significantly robust west of 60°E from October to December. The 2010 summer heatwave that affected Western Europe and Russia was due to the long-term (>1 month) persistence of Ural blocking [*Barriopedro et al.*, 2011; *Matsueda*, 2011]. All the ΔSST

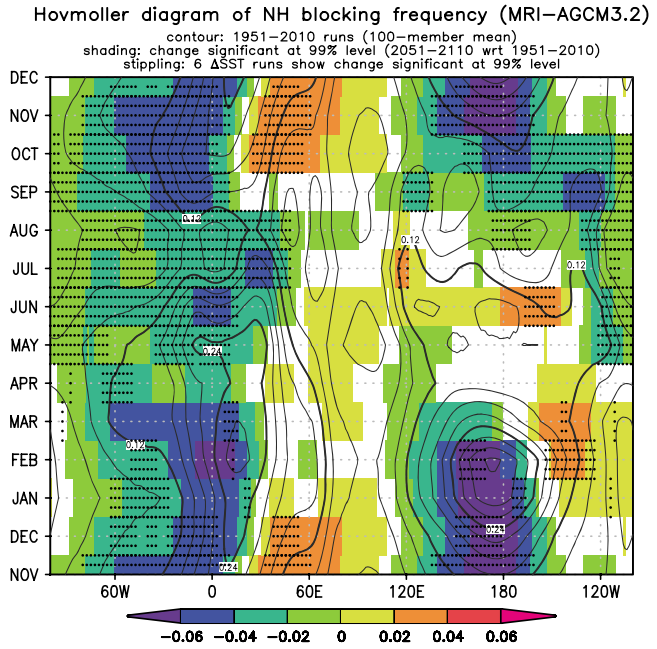

Figure 4. Hovmöller diagram of the simulated blocking frequency over the Northern Hemisphere for the period 1951–2010 (100-member mean, contours) and significant change (at the 99% confidence level) for 2051–2110 relative to 1951–2010 (shading). Significance values are based on 100- and 90-member ensembles for the periods 1951–2010 and 2051–2110, respectively. The stippled areas indicate that all ΔSST ensemble simulations show significant changes in blocking frequency at the 99% confidence level, compared with the corresponding 100-member mean frequency for the period 1951–2010.

ensemble simulations (except the MRI-CGC3 SST-forced simulations) show an increased frequency of Ural blocking in June only (Figure S5).

In the Pacific sector, our simulations depict significant and robust declines in blocking frequency, mainly in late summer and early spring. However, the largest reduction (January–February) exhibits a weaker robustness owing to the relatively weak signals in the CCSM4 SST-forced simulations, for which the El Niño signal is also the weakest (Figure 1).

Projected wintertime reductions over the Euro-Atlantic and Pacific sectors are consistent with previous studies [e.g., *Matsueda et al.*, 2009; *Masato et al.*, 2013]. We also observed significant and robust increases in blocking frequency around 120°E in July, 140°W in late winter-early spring, and 160°W in June, along with a significant but less robust increase between 100°E and 180°E. We speculate that the July increase around 120°E may serve to enhance the development of the surface Okhotsk High, which brings northeasterly surface winds and anomalously cold and cloudy summers to northeast Japan [*Nakamura and Fukamachi*, 2004].

4. Summary and Conclusions

We used the high-resolution MRI-AGCM3.2 model, prescribed with six CMIP5-derived future SST patterns to conduct large-ensemble simulations of Northern Hemisphere blocking events in a climate 4 K warmer than preindustrial time. As summarized below, intrinsic differences in the prescribed future SST warming resulted in either consistent or inconsistent responses of blocking activity to global warming among the simulations.

During the Pacific winter, all model runs projected significant and robust decreases in the frequency of blocking events, with the areal-mean frequency declining from 17.4% ± 0.7% to 14.8% ± 2.4%. The stronger the canonical El Niño-like SST warming, the larger the decrease in frequency over the peak's western tail. The CP El Niño-like SST warming also leads to a similar reduced frequency of blocking. In addition, the number of Pacific blocking events exceeding 15 days' duration is significantly and robustly reduced, whereas events lasting 5–9 and 10–14 days exhibit a significant but nonrobust increase and decrease, respectively. No simulation projected a decrease in the number of blocking events lasting between 5 and 9 days.

In the Euro-Atlantic sector, the projected frequency of wintertime blocking events also exhibits a significant and robust decline, with the areal-mean frequency dropping from 16.6% ± 0.7% to 13.1% ± 2.1%. In contrast to the Pacific sector, significant and robust reductions occurred regardless of event duration. The reduction in blocking frequency is relatively insensitive to the strength of the canonical El Niño signal. In contrast, the CP El Niño-like SST warming results in a similar or increased frequency of Euro-Atlantic blocking events compared with the historical climate, especially over continental Europe. Given that CP El Niño events could become more frequent in a warming climate [*Yeh et al.*, 2009], we cannot exclude the possibility of slightly increased frequencies of Euro-Atlantic blocking.

During the Euro-Atlantic summer months, all ΔSST ensemble simulations show a significant reduction in blocking frequency east of 50°E, consistent with previous studies [e.g., *Masato et al.*, 2013]. The areal-mean frequency declines from 10.7% ± 0.4% to 7.6% ± 0.7%. We also observed a significant and robust decrease in the number of events lasting up to 24 days. However, the longer the blocking duration, the less robust the decrease in the number of events. In the Ural sector, the majority of simulations projected a frequency similar to current climate conditions. Considering the anticipated rise in future surface temperature, Europe and east Russia may potentially experience more severe heatwaves due to long-lasting blocking events.

Summertime blocking frequency in the Pacific sector is projected either to remain unchanged or to increase slightly. For example, while several models project a higher frequency of blocking events lasting between 15 and 29 days, the scale of these changes is minor. We suggest that this unique response of Pacific summertime blocking to global warming indicates the influence of mechanisms other than season and region, such as intensified land-sea thermal contrast [*Arai and Kimoto*, 2008; *Kamae et al.*, 2014]. This problem deserves further study.

Acknowledgments
This work was performed under the Development of Basic Technology for Risk Information on Climate Change of the SOUSEI Program of the Ministry of Education, Culture, Sports, Science and Technology (MEXT) of Japan. Model integrations were performed using the Earth Simulator. The d4PDF ensemble data sets used here are available at the Data Integration and Analysis System Program (DIAS) database (http://www.miroc-gcm.jp/~pub/d4PDF/design_en.html). The authors thank two anonymous reviewers for their useful comments.

References

Anstey, J. A., P. Davini, L. J. Gray, T. J. Woollings, N. Butchart, C. Cagnazzo, B. Christiansen, S. C. Hardiman, S. M. Osprey, and S. Yang (2013), Multi-model analysis of Northern Hemisphere winter blocking: Model biases and the role of resolution, *J. Geophys. Res. Atmos.*, *118*, 3956–3971, doi:10.1002/jgrd.50231.

Arai, M., and M. Kimoto (2008), Simulated interannual variation in summertime atmospheric circulation associated with the East Asian monsoon, *Clim. Dyn.*, *31*, 435–447, doi:10.1007/s00382-007-0317-y.

Barriopedro, D., E. M. Fischer, J. Luterbacher, R. M. Trigo, and R. García-Herrera (2011), The hot summer of 2010: Redrawing the temperature record map of Europe, *Science*, *332*, 220–224, doi:10.1126/science.1201224.

Black, E., M. Blackburn, G. Harrison, B. Hoskins, and J. Methven (2004), Factors contributing to the summer 2003 European heatwave, *Weather*, *59*, 217–223, doi:10.1256/wea.74.04.

Bourke, R. H., and R. P. Garrett (1987), Sea ice thickness distribution in the Arctic Ocean, *Cold Reg. Sci. Technol.*, *13*(3), 259–280, doi:10.1016/0165-232X(87)90007-3.

D'Andrea, F., et al. (1998), Northern Hemisphere atmospheric blocking as simulated by 15 atmospheric general circulation models in the period 1979–1988, *Clim. Dyn.*, *14*, 385–407, doi:10.1007/s003820050230.

Davini, P., and F. D'Andrea (2016), Northern Hemisphere atmospheric blocking representation in global climate models: Twenty years of improvements?, *J. Clim.*, *29*, 8823–8840, doi:10.1175/JCLI-D-16-0242.1.

Graf, H.-F., and D. Zanchettin (2012), Central Pacific El Niño, the "subtropical bridge," and Eurasian climate, *J. Geophys. Res.*, *117*, D01102, doi:10.1029/2011JD016493.

Hirahara, S., M. Ishii, and Y. Fukuca (2014), Centennial-scale sea surface temperature analysis and its uncertainty, *J. Clim.*, *27*, 57–75, doi:10.1175/JCLI-D-12-00837.1.

Intergovernmental Panel on Climate Change (IPCC) (2013), in *Climate Change 2013: The Physical Science Basis. Contribution of Working Group I to the Fifth Assessment Report of the Intergovernmental Panel on Climate Change*, edited by T. F. Stocker et al., pp. 1207–1308, Cambridge Univ. Press, Cambridge, U. K., and New York.

Jung, T., et al. (2012), High-resolution global climate simulations with the ECMWF model in Project Athena: Experimental design, model climate, and seasonal forecast skill, *J. Clim.*, *25*, 3155–3172, doi:10.1175/JCLI-D-11-00265.1.

Kamae, Y., M. Watanabe, M. Kimoto, and H. Shiogama (2014), Summertime land-sea thermal contrast and atmospheric circulation over East Asia in a warming climate—Part I: Past changes and future projections, *Clim. Dyn.*, *43*, 2553–2568, doi:10.1007/s00382-014-2073-0.

Kobayashi, S., et al. (2015), The JRA-55 reanalysis: General specifications and basic characteristics, *J. Metorol. Soc. Jpn.*, *93*, 5–48, doi:10.2151/jmsj.2015-001.

Masato, G., B. J. Hoskins, and T. Woollings (2013), Winter and summer Northern Hemisphere blocking in CMIP5 models, *J. Clim.*, *26*, 7044–7059, doi:10.1175/JCLI-D-12-00466.1.

Matsueda, M. (2011), Predictability of Euro-Russian blocking in summer of 2010, *Geophys. Res. Lett.*, *38*, L06801, doi:10.1029/2010GL046557.

Matsueda, M., R. Mizuta, and S. Kusunoki (2009), Future change in wintertime atmospheric blocking simulated using a 20-km-mesh atmospheric global circulation model, *J. Geophys. Res.*, *114*, D12114, doi:10.1029/2009JD011919.

Matsueda, M., H. Endo, and R. Mizuta (2010), Future change in Southern Hemisphere summertime and wintertime atmospheric blockings simulated using a 20-km-mesh AGCM, *Geophys. Res. Lett.*, *37*, L02803, doi:10.1029/2009GL041758.

Meehl, G. A., C. Covey, T. Delworth, M. Latif, B. McAvaney, J. F. B. Mitchell, R. J. Stouffer, and K. E. Taylor (2007), The WCRP CMIP3 multimodel dataset: A new era in climate change research, *Bull. Am. Meteorol. Soc.*, *88*, 1383–1394, doi:10.1175/BAMS-88-9-1383.

Mizuta, R., et al. (2012), Climate simulations using MRI-AGCM3.2 with 20-km grid, *J. Meteorol. Soc. Jpn.*, *90A*, 233–258, doi:10.2151/jmsj.2012-A12.

Mizuta, R., O. Arakawa, T. Ose, S. Kusunoki, H. Endo, and A. Kitoh (2014), Classification of CMIP5 future climate responses by the tropical sea surface temperature changes, *SOLA*, *10*, 167–171, doi:10.2151/sola.2014-035.

Mizuta, R., et al. (2017), Over 5000 years of ensemble future climate simulation by 60 km global and 20 km regional atmospheric models, *Bull. Am. Meteorol. Soc.*, doi:10.1175/BAMS-D-16-0099.1.

Nakamura, H., and T. Fukamachi (2004), Evolution and dynamics of summertime blocking over the Far East and the associated surface Okhotsk high, *Q. J. R. Meteorol. Soc.*, *130*, 1213–1233, doi:10.1256/qj.03.101.

Palmer, T. N., F. J. Doblas-Reyes, A. Weisheimer, and M. J. Rodwell (2008), Toward seamless prediction: Calibration of climate change projections using seasonal forecasts, *Bull. Am. Meteorol. Soc.*, *89*, 459–470, doi:10.1175/BAMS-89-4-459.

Palmer, T. N., and D. A. Mansfield (1984), Response of two atmospheric general circulation models to sea-surface temperature anomalies in the tropical East and West Pacific, *Nature*, *310*, 483–485, doi:10.1038/310483a0.

Schiemann, R., M.-E. Demory, L. C. Shaffrey, J. Strachan, P. L. Vidale, M. S. Mizielinski, M. J. Roberts, M. Matsueda, M. F. Wehner, and T. Jung (2017), The resolution sensitivity of Northern Hemisphere blocking in four 25-km atmospheric global circulation models, *J. Clim.*, *30*, 337–358, doi:10.1175/JCLI-D-16-0100.1.

Taylor, K. E., R. J. Stouffer, and G. A. Meehl (2012), An overview of CMIP5 and the experiment design, *Bull. Am. Meteorol. Soc.*, *93*, 485–498, doi:10.1175/BAMS-D-11-00094.1.

Trenberth, K. E., J. T. Fasullo, G. Branstator, and A. S. Phillips (2014), Seasonal aspects of the recent pause in surface warming, *Nat. Clim. Change*, *4*, 911–916, doi:10.1038/nclimate2341.

Yeh, S.-W., J.-S. Kug, B. Dewitte, M.-H. K. B. P. Kirtman, and F.-F. Jin (2009), El Niño in a changing climate, *Nature*, *461*, 511–514, doi:10.1038/nature0831.

Geophysical Research Letters

Supporting Information for

The robustness of future changes in Northern Hemisphere blocking: a large ensemble projection with multiple sea surface temperature patterns

Mio Matsueda[1,2] and Hirokazu Endo[3]

[1]Center for Computational Sciences, University of Tsukuba, Tsukuba, Japan

[2]Department of Physics, University of Oxford, Oxford, UK

[3]Meteorological Research Institute, Tsukuba, Japan

Contents of this file

Figures S1 to S5

Introduction

This supporting Information includes the following figures:

- Projected frequency of blocking in winter for all the models (Fig. S1);
- Projected future changes of geopotential height at 500hPa in winter for all the models (Fig. S2);
- Projected future changes of precipitation and velocity potential at 200hPa in winter for all the models (Fig. S3);
- Projected frequency of blocking in summer for all the models (Fig. S4);
- Hovmöller diagram of projected frequency of blocking over the Northern Hemisphere (Fig. S5).

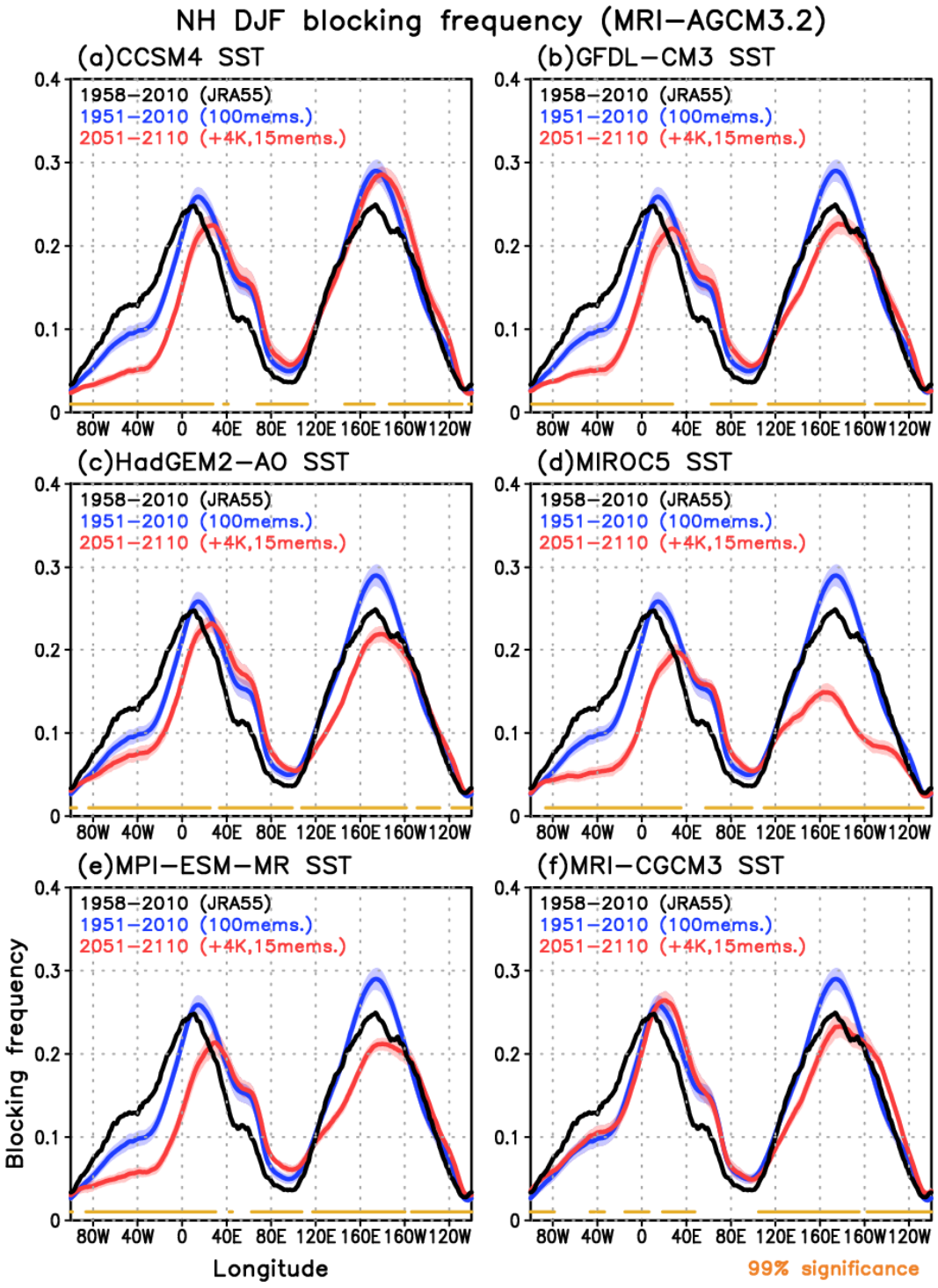

Figure S1. As for Figure 2a, but for each ΔSST ensemble simulation with SSTs from (a) CCSM4, (a) CCSM4, (b) GFDL-CM3, (c) HadGEM2-AO, (d) MIROC5, (e) MPI-ESM-MR, and (f) MRI-CGCM3.

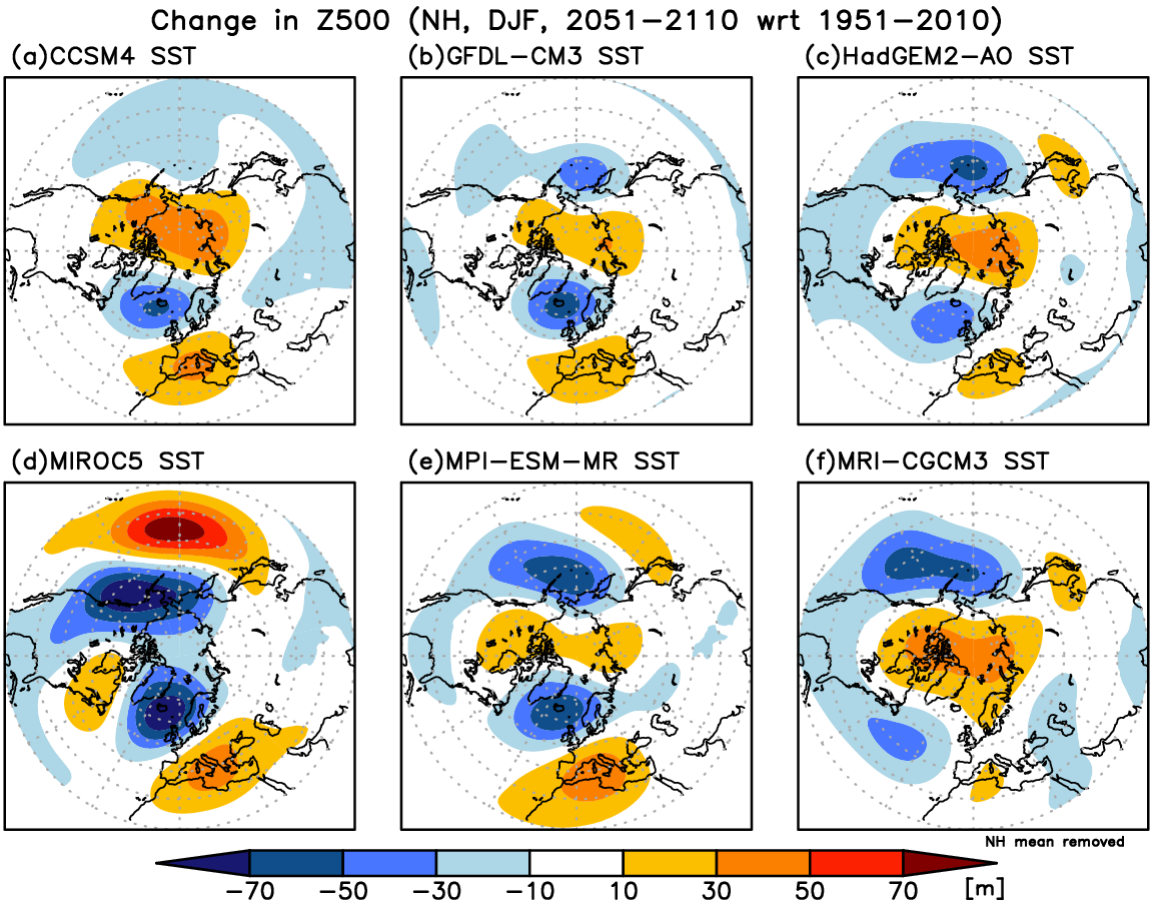

Figure S2. Ensemble-mean DJF climate-change signals of Z500 for the ΔSST simulations prescribed with SSTs from (a) CCSM4, (b) GFDL-CM3, (c) HadGEM2-AO, (d) MIROC5, (e) MPI-ESM-MR, and (f) MRI-CGCM3. The hemispheric mean has been removed.

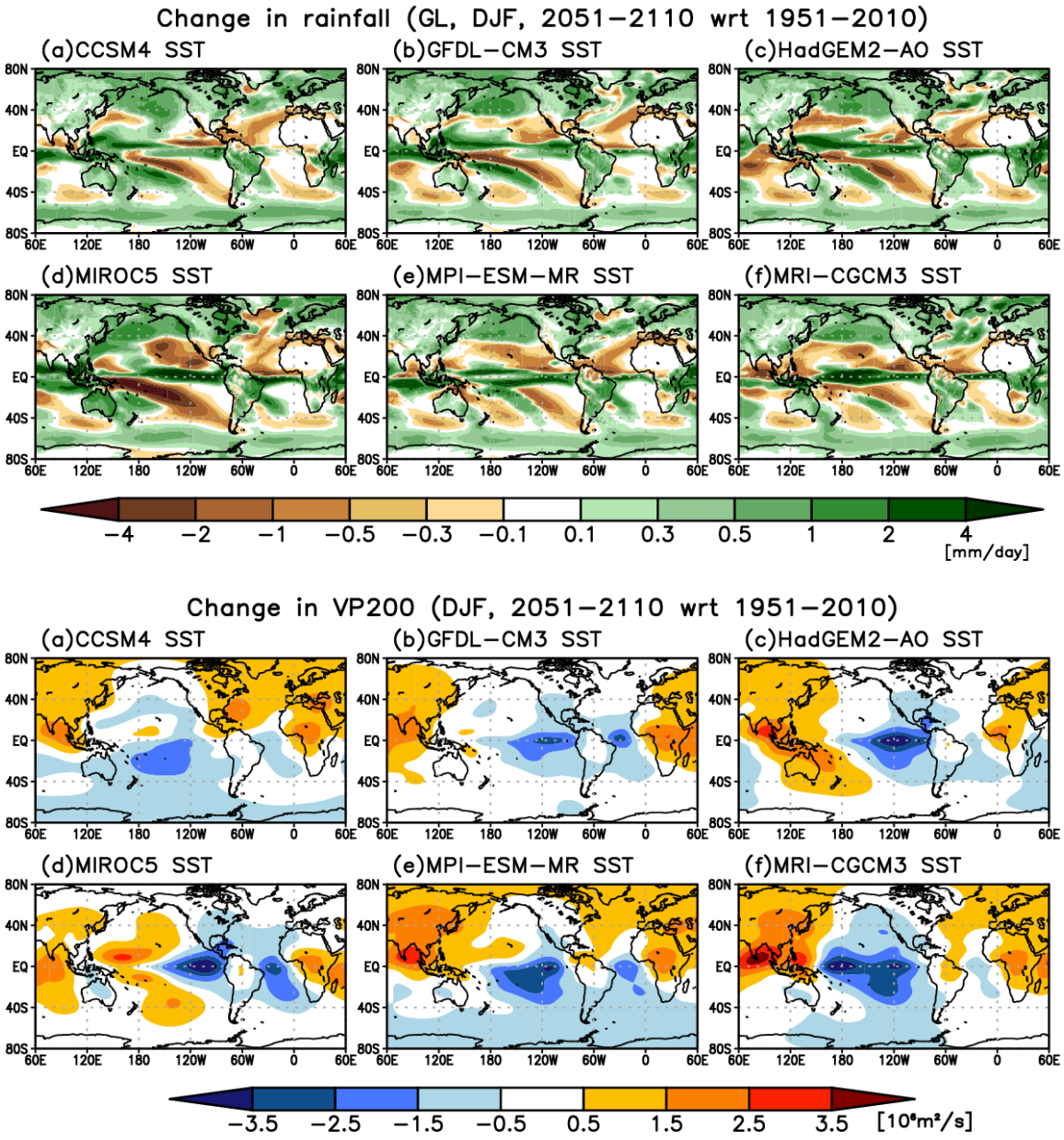

Figure S3. Projected future changes in (top, a–f) precipitation and (bottom, a–f) velocity potential at 200 hPa in DJF for each ΔSST ensemble simulation prescribed with SSTs from (a) CCSM4, (b) GFDL-CM3, (c) HadGEM2-AO, (d) MIROC5, (e) MPI-ESM-MR, and (f) MRI-CGCM3.

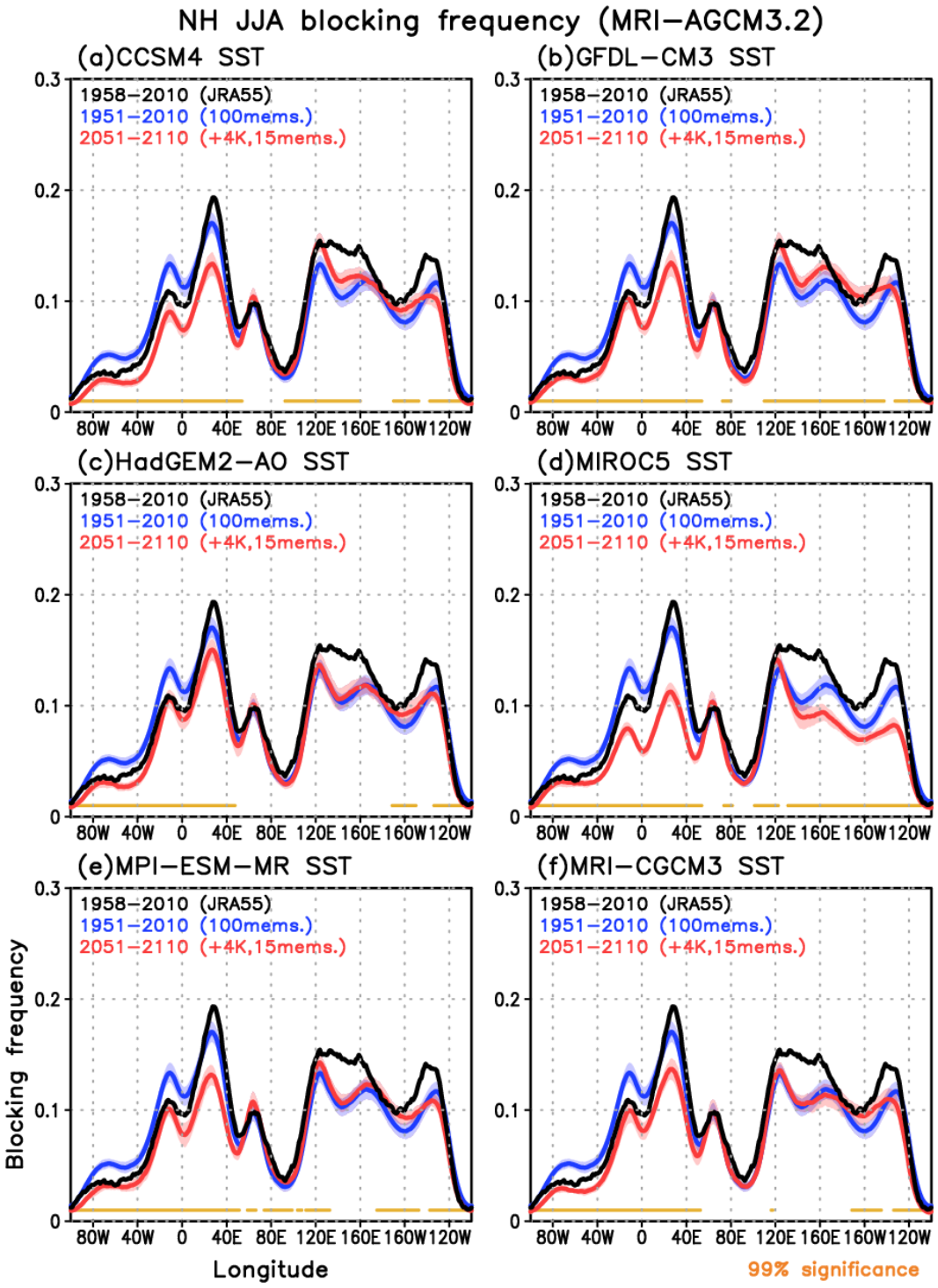

Figure S4. As for Figure S1, but for summer (JJA).

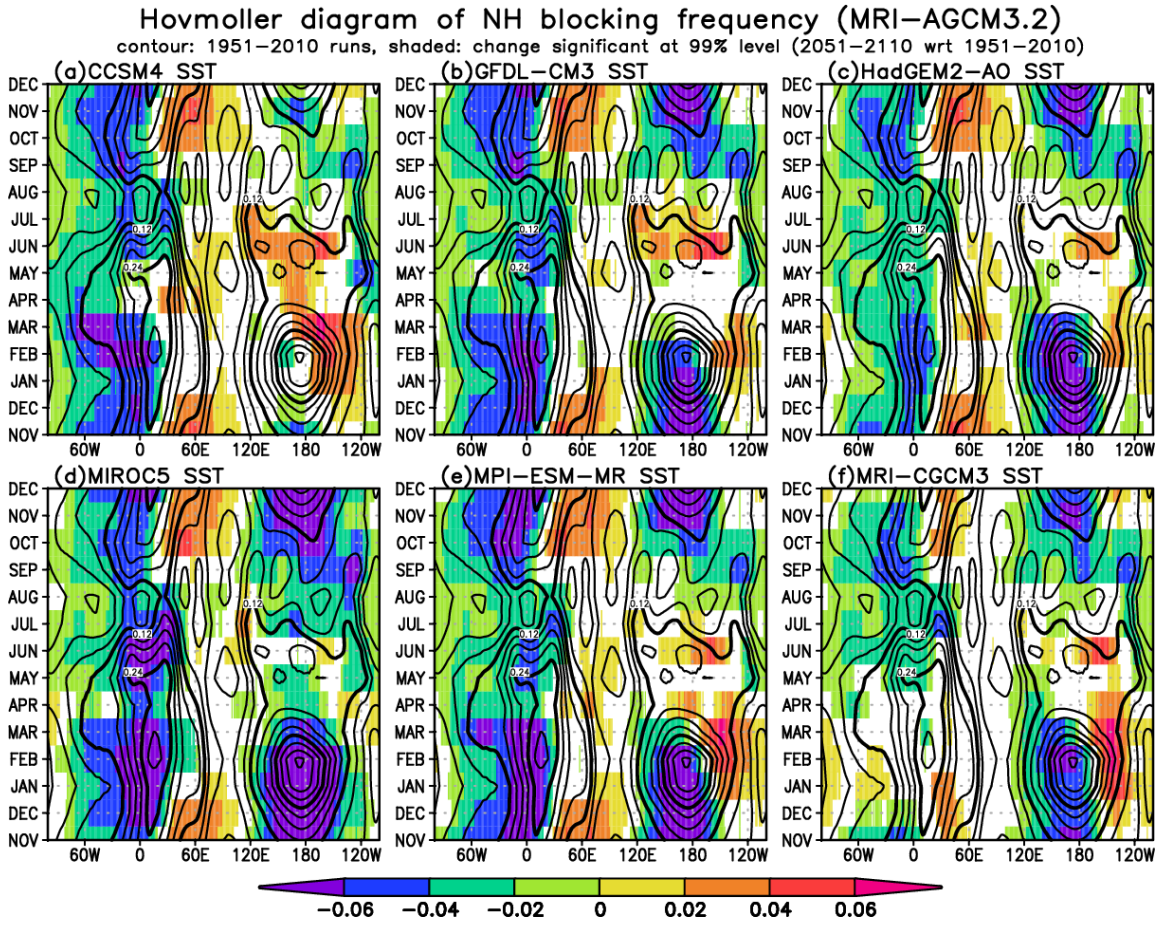

Figure S5. Hovmöller diagram of (contours) the simulated blocking frequency over the Northern Hemisphere for the period 1951–2010, and (shading) its significant change (at the 99% confidence level) in 2051–2110 relative to 1951–2010, for each ΔSST ensemble simulation prescribed with SSTs from (a) CCSM4, (b) GFDL-CM3, (c) HadGEM2-AO, (d) MIROC5, (e) MPI-ESM-MR, and (f) MRI-CGCM3. Significance values are based on 100- and 15-member ensembles for the periods 1951–2010 and 2051–2110, respectively.